Topics in Catalysis
https://doi.org/10.1007/s11244-024-02007-6

ORIGINAL PAPER

Synthesis of α,ω-Primary Hydroxyl-Terminated Polyether Polyols Using Prussian Blue Analogs as Catalysts

Chinh Hoang Tran[1,2] · Byeong-Ryeol Moon[1] · Ju-Yeong Heo[1] · So-Young Kim[1] · Ji-Hwan Park[1] · Won-Seok Jae[1] · Il Kim[1]

Accepted: 19 August 2024

Abstract
Polyalkylene oxides and polyether polyols are the most frequently used raw materials in polyurethane production, and are commonly produced via the ring-opening polymerization of epoxides, particularly propylene oxide. However, the resulting polyols predominantly contain predominantly secondary hydroxyl groups (up to 95%) that are less reactive than those capped with primary hydroxyl groups, thereby limiting the applications of the former in polyurethane synthesis. In this study, a viable procedure for producing α,ω-primary hydroxyl-terminated polyols using various Prussian blue analogs as heterogeneous catalysts was developed. The reaction kinetics were first investigated to gain insight into the reactivity of primary and secondary alcohols in the ring-opening of ε-caprolactone. Subsequently, ε-caprolactone-capped polyols with predominantly primary hydroxyl groups were successfully synthesized via the ring-opening reaction of ε-caprolactone using polypropylene glycol as the macroinitiator. The reactivities of the resultant ε-caprolactone-capped polyols for polyurethane synthesis were greatly enhanced compared to those of conventional polyols.

Keywords Prussian blue analogs · Double metal cyanide · Polyether polyol · Ring-opening polymerization

1 Introduction

Polyurethane (PU) was discovered by Otto Bayer, a German chemist, and his coworkers in 1937 [1, 2]. PU materials are employed as alternatives to nylon and rubber because of their excellent mechanical properties, such as surface stability, flexibility, and adhesiveness [3–10]. PU materials are currently used in a wide range of applications in manufacturing and daily life, with a global market volume of over 25 million tons and a market value of approximately 65 billion USD [11, 12]. PUs are generally produced by reacting isocyanates with polyols, where the characteristics of the polyols, such as their hydroxyl functionalities, molecular weights (MWs), and terminal hydroxyl groups, have crucial effects on the chemical and physical properties, as well as the performances of the end products [13].

Polypropylene glycols (PPGs) derived from propylene oxide are the most widely used precursors in PU manufacturing because of their versatility and abundance. PPGs are commercially produced via anionic ring-opening polymerization of propylene oxide using basic catalysts (e.g., KOH) [14]. The ring-opening of propylene oxide can proceed via both α- and β-cleavage routes; however, in base-catalyzed

✉ Il Kim
ilkim@pusan.ac.kr

Chinh Hoang Tran
chinhtran@pusan.ac.kr

Byeong-Ryeol Moon
moonbro@pusan.ac.kr

Ju-Yeong Heo
hjy0496@pusan.ac.kr

So-Young Kim
ksy906@pusan.ac.kr

Ji-Hwan Park
wlghks1704@pusan.ac.kr

Won-Seok Jae
coly2343@pusan.ac.kr

[1] School of Chemical Engineering, Pusan National University, Busandaehag-ro 63-2, Geumjeong-gu, Busan 46241, Republic of Korea

[2] Institute of Applied Materials Science, Vietnam Academy of Science and Technology, TL29 Street, District 12, Ho Chi Minh 70000, Vietnam

Published online: 03 September 2024

anionic polymerization, β-cleavage of the epoxy ring is favored, resulting in PPGs with predominant secondary hydroxyl groups (up to 95%). Furthermore, basic catalysts can produce PPGs with significant monol contents or unsaturation values. These factors significantly affect the performance of PPG polyols in PU synthesis [15].

Considerable effort has been devoted to increasing the primary –OH content of the final PPG products and diminishing their monol contents. Especially, Lewis acid catalytic systems and double metal cyanide (DMC) catalysts have been explored [16–19]. Lewis-acid-mediated systems, such as boron compounds, can be used to afford PPG polyols with significant primary hydroxyl contents compared to those of the secondary congeners (50–70%). However, these catalytic systems are rarely used in PPG production because of their relatively high costs, difficulty in handling, and the possibility of side reactions. DMC compounds are well-known catalysts that are used industrially to produce high-quality PPG polyols with extremely low contents of unsaturated impurities. However, polyether polyols produced via DMC catalysis contain few primary –OH groups [20].

Another approach for increasing the primary –OH contents of PPG polyols is via post-synthesis modification of PPG by ethylene oxide end-capping using KOH or by propylene oxide end-capping wherein DMC and Lewis acidic boron compounds are combined in a dual catalytic system [21, 22]. DMC belongs to one of the oldest classes of inorganic complexes, also known as Prussian blue analogs (PBAs). These complexes have been employed in various fields such as catalysis [23–31], battery materials [32–41], biomedical applications [42–44], electrochemical sensors [45–47], and sorbents [48, 49]. Recently, we found that PBAs effectively catalyze the ring-opening of lactones using both monoinitiators and macroinitiators [50], which motivated us to investigate these complexes for the synthesis of lactone-capped PPG polyols.

In this study, a series of PBA catalysts is prepared in the absence of organic complexing agents using various central metal atoms (Co, Fe, Mn, and Zn). The activities of the as-prepared catalysts are evaluated for the ring-opening of ε-caprolactone (CL) using ethylene glycol (EG) as an initiator. Kinetic studies are conducted using a propylene glycol initiator to gain insight into the reactivity of the primary and secondary hydroxyl groups in the ring-opening of CL, paving the way for the synthesis of CL-capped PPG polyols. To highlight the advantages of the current approach, the reactivities of the resulting CL-capped polyols for PU synthesis are evaluated and compared with those of conventional PPG.

2 Materials and methods

2.1 Materials

Potassium hexacyanocobaltate(III) ($K_3Co(CN)_6$, ≥97%) and hexamethylene diisocyanate (HDI, ≥98%) were purchased from Merck Korea (Seoul, Korea). Phosphoric acid (≥89%) was purchased from Tokyo Chemical Industry Co., Ltd. (Incheon, Korea). Zinc(II) chloride anhydrous (≥98%), ethylene glycol (EG, 99%), and ε-caprolactone (CL, 99%) were obtained from Fisher Scientific Korea (Incheon, Korea). Nitric acid (60–62%) was purchased from Junsei Chemical Co., Ltd. (Tokyo, Japan). Potassium cyanide (≥97.5%) was obtained from Duksan Pure Chemicals (Incheon, Korea). Manganese(II) chloride tetrahydrate (≥98%) and propylene glycol (PG, ≥99.5%) were purchased from DaeJung Chemical Co. (Gyeonggi-do, Korea). PPG (MW: 500, functionality: 2) was obtained from Kumho Petrochemical Co. (Ulsan, Korea). Propylene oxide was obtained from SKC Polyurethanes, Inc. (Ulsan, Korea). EG, PG, and PPG were distilled prior to use. Potassium manganese cyanide ($K_3Mn(CN)_6$) was prepared according to literature methods, recrystallized in warm 10% potassium cyanide solution, and dried before use [51]. Unless otherwise mentioned, all other reagents were used without further purification.

2.2 Catalyst Preparation

The PBA catalysts were prepared by mixing an aqueous solution of a metal salt with a metal cyanide salt. A stoichiometric ratio of the metal salt to metal cyanide salt was used to ensure the formation of PBAs with the desired composition. As an example, a solution of $ZnCl_2$ (0.31 g, 2.28 mmol) in distilled water (2.5 mL) was added to a solution of $K_3Mn(CN)_6$ (0.5 g, 1.52 mmol) in distilled water (2.5 mL) under vigorous stirring at 25 °C. The resulting precipitate was washed with 10 mL distilled water and dried to produce $Zn_3[Mn(CN)_6]_2$. $Zn_3[Co(CN)_6]_2$ and $Mn_3[Mn(CN)_6]_2$ were prepared using the same method.

2.3 Catalytic Reaction

All reactions were performed using standard Schlenk techniques. For the ring-opening reaction of CL, prescribed amounts of the PBA catalyst and hydroxyl-containing initiator were added to a 10 mL round-bottom flask, which was then immersed in an oil bath and heated to 90 °C under nitrogen flow for 30 min to remove traces of water. The temperature was raised to 160 °C, and prescribed amounts of CL were added under continuous stirring. Occasionally,

small amounts of the reaction mixture were collected for further analysis.

Using a 50 mL round-bottom flask, the reactions of polyols with HDI was investigated. Typically, a prescribed amount of polyol was added to the reactor and purged with nitrogen for 30 min at 90 °C to remove traces of water. The reactor was then cooled to 60 °C, and the prescribed amount of HDI was added under vigorous stirring and the resulting mixture was allowed to react for 3 h, and samples of the reaction mixture were collected at different intervals to determine the conversion of –NCO groups by Fourier-transform infrared (FTIR) analysis.

2.4 Characterization

FTIR data were acquired using a Shimadzu IR Prestige 21 spectrometer (Shimadzu Co., Tokyo, Japan). The crystal structures of the catalysts were determined using a RINT2000 wide-angle diffractometer (Rigaku Co., Tokyo, Japan) equipped with a 185 mm radius goniometer and Cu-Kα radiation. The morphologies and particle sizes of the catalysts were investigated by scanning electron microscopy (SEM) using an S-3000 H microscope (Hitachi Ltd., Tokyo, Japan). Nuclear magnetic resonance (NMR) analysis was conducted using an INOVA 400 NMR spectrometer (Varian Inc., California, USA). Chemical shifts are presented as parts per million (ppm) relative to the peaks of the residual monomer used as the internal standard. Gel permeation chromatography (GPC) was performed using a Waters 150 instrument (Agilent Technologies, Santa Clara, California, USA). Tetrahydrofuran was used as the diluent at a flow rate of 1 mL min^{-1}, at 40 °C, and polystyrene was used as the standard for calibration.

3 Results and Discussion

3.1 Catalyst Characterization

Figure 1a and Supplementary Fig. S1 show the FTIR spectra of the prepared PBA catalysts. The characteristic signals corresponding to the C≡N stretching vibrations of $Zn_3[Co(CN)_6]_2$, $Zn_3[Mn(CN)_6]_2$, and $Mn_3[Mn(CN)_6]_2$ were observed at approximately 2184, 2220, and 2146 cm^{-1}, respectively. Additionally, signals attributed to the metal − CN bending vibrations were located at approximately 454, 466, and 503 cm^{-1}, respectively. The variations in the intensities and positions of these characteristic peaks provide insight into how the different central metal atoms (i.e., Zn, Co, and Mn) interact with cyanide in each PBA. The broad peaks at approximately 3550–3000 and 1680–1590 cm^{-1} are attributed to the –OH stretching vibrations and H–O–H deformation of the physisorbed water involved in a hydrogen-bonded network [52]. In contrast, the sharp peaks at approximately 3700–3550 cm^{-1} are assigned to the –OH stretching vibrations of chemisorbed water molecules involved in metal–OH coordination [30]. The results of the FTIR analysis are presented in Supplementary Table S1.

The crystal structures and crystal phases of the as-prepared PBAs were determined using X-ray diffraction (XRD) analysis. As shown in Fig. 1b and Supplementary Fig. S2, the $Zn_3[Co(CN)_6]_2$, $Co_3[Mn(CN)_6]_2$, $Fe_3[Mn(CN)_6]_2$, and $Mn_3[Mn(CN)_6]_2$ compounds exhibited a pure face-centered cubic structure (space group *Fm*-3*m*) with characteristic reflection peaks corresponding to the (111), (200), (220), (400), (420), (422), (440), (600), and (620) planes. Meanwhile, $Zn_3[Mn(CN)_6]_2$ exhibited a monoclinic structure in the *Pn*-3*m* space group, with reflections corresponding to specified planes at $2\theta = 21.3°$ (011), 26.0° (111), 37.2° (112), 43.4° (022), 48.8° (013), and 58.5° (123). The differences in the coordination environments of the central metal atoms had a noticeable impact on the crystalline structure and size of the catalyst clusters, as evidenced by the variations in the intensity and position of these characteristic reflections.

The thermal stability of the PBA catalysts was determined using thermogravimetric analysis (TGA) (Fig. 1c and Supplementary Fig. S3). All catalysts exhibited two-stage decomposition curves corresponding to the decomposition of the absorbed water and –C≡N– bonds. $Zn_3[Co(CN)_6]_2$ exhibited the highest thermal stability, completely decomposing at approximately 550 °C, which is much higher than the decomposition temperature of $Zn_3[Mn(CN)_6]_2$ (approximately 370 °C) and $Mn_3[Mn(CN)_6]_2$ (approximately 200 °C). The amount of absorbed water in the PBA catalysts decreased in the order: $Zn_3[Co(CN)_6]_2$ (11.6%) > $Mn_3[Mn(CN)_6]_2$ (6.8%) > $Zn_3[Mn(CN)_6]_2$ (2.2%), which is in good agreement with the FTIR data.

The morphologies and particle sizes of the catalysts were determined using SEM. As shown in Fig. 1d and Supplementary Fig. S4, $Zn_3[Co(CN)_6]_2$ formed highly crystalline cubic particles (approximately 513.2 nm). The particle size of PBA decreased significantly when the central Co atom was replaced by Mn, as observed for $Co_3[Mn(CN)_6]_2$ (56.7 nm), $Fe_3[Mn(CN)_6]_2$ (63.5 nm), $Zn_3[Mn(CN)_6]_2$ (53.3 nm), and $Mn_3[Mn(CN)_6]_2$ (21.4 nm). Additionally, the edges of $Zn_3[Mn(CN)_6]_2$ and $Mn_3[Mn(CN)_6]_2$ underwent a significant shape transformation compared to those of $Zn_3[Co(CN)_6]_2$, with slight debris on the plane surface, likely due to the dissociation of $[Mn(CN)_6]^{-3}$ and etching of the resulting PB crystal. The characterization data for the PBA catalysts are presented in Table 1.

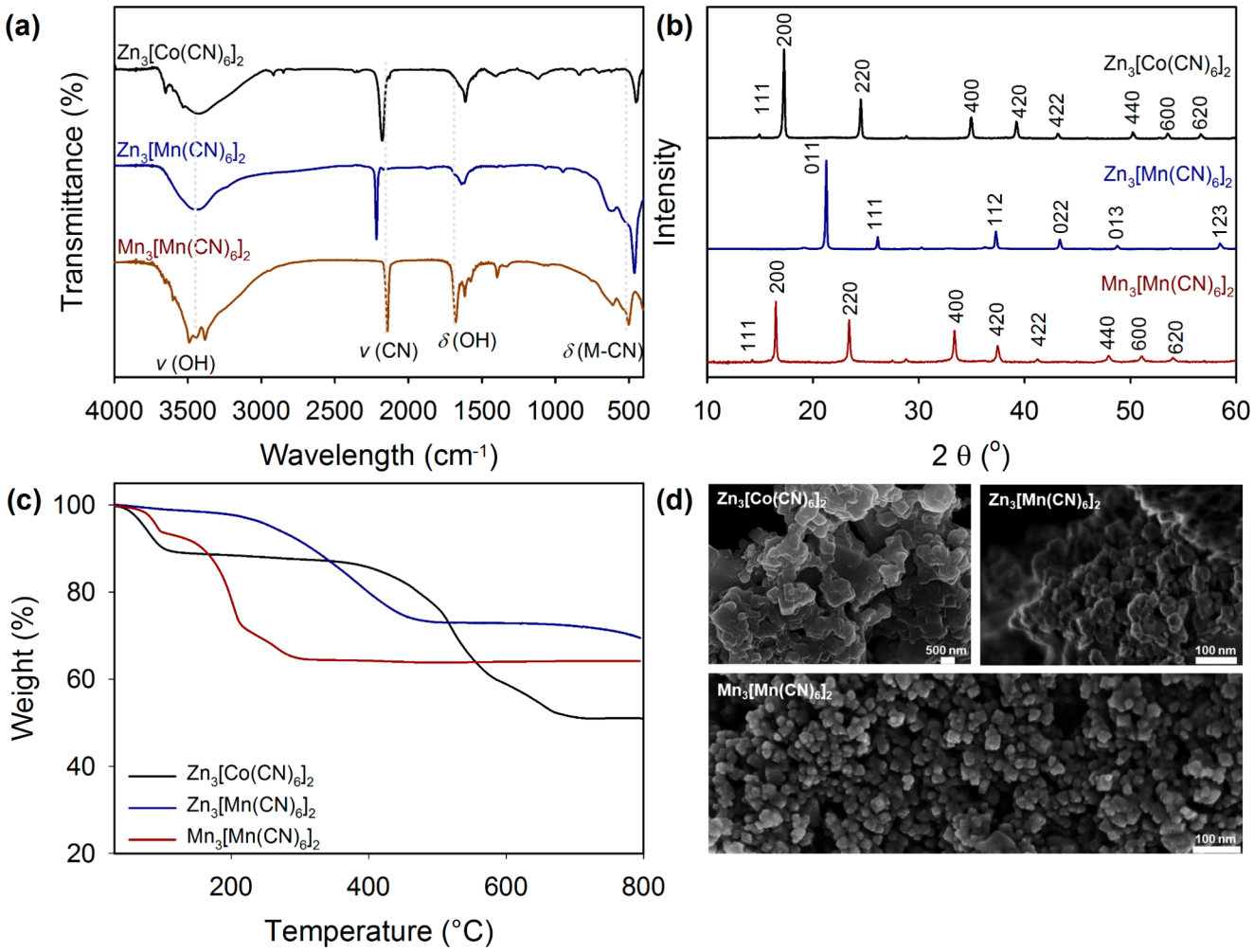

Fig. 1 Characterization of the representative PBA catalysts: (**a**) FTIR spectra, (**b**) XRD patterns, (**c**) TGA curves, (**d**) SEM images

Table 1 Structural properties of the representative PBA catalysts

Catalyst	CN (%)	H_2O (%)	Space group	Lattice constants (Å)	Crystal structure	Crystallite size (nm)
$Zn_3[Co(CN)_6]_2$	36.9	11.6	*Fm*-3*m*	$a=b=c=10.26$	Cubic	513.2
$Zn_3[Mn(CN)_6]_2$	24.5	2.2	*Pn*-3*m*	$a=b=c=5.90$	Monoclinic	53.3
$Mn_3[Mn(CN)_6]_2$	29.4	6.8	*Fm*-3*m*	$a=b=c=10.73$	Cubic	21.4

3.2 Catalyst Screening

The activity of the PBA catalysts was first investigated in the ring-opening of CL using EG as the hydroxyl initiator (Fig. 2). The reactions were conducted under a nitrogen atmosphere at 160 °C for 3 h, and the crude reaction mixture was analyzed at different intervals from 0.5 to 3 h using ^{1}H NMR. The conversion of CL was determined based on the integration of the signals related to the methylene protons of CL at approximately 1.75, 1.84, 2.63, and 4.21 ppm (Supplementary Figs. S5–S15). The control reaction, which was performed in the absence of a catalyst, indicated negligible conversion of CL, and no adducts were observed. Among the catalysts, only $Mn_3[Mn(CN)_6]_2$ and $Zn_3[Mn(CN)_6]_2$ showed remarkable activity for the ring-opening of CL, whereas the other PBA catalysts exhibited relatively low activity (maximum CL conversion of 36% after 3 h). The $Mn_3[Mn(CN)_6]_2$ catalyst exhibited the highest activity, achieving > 90% CL conversion after 30 min, whereas $Zn_3[Mn(CN)_6]_2$ required 3 h to achieve a similar CL conversion.

3.3 Kinetics of the ring-opening of CL Using $Mn_3[Mn(CN)_6]_2$

Kinetic studies were conducted using the $Mn_3[Mn(CN)_6]_2$ catalyst to evaluate the reactivity of the primary and secondary

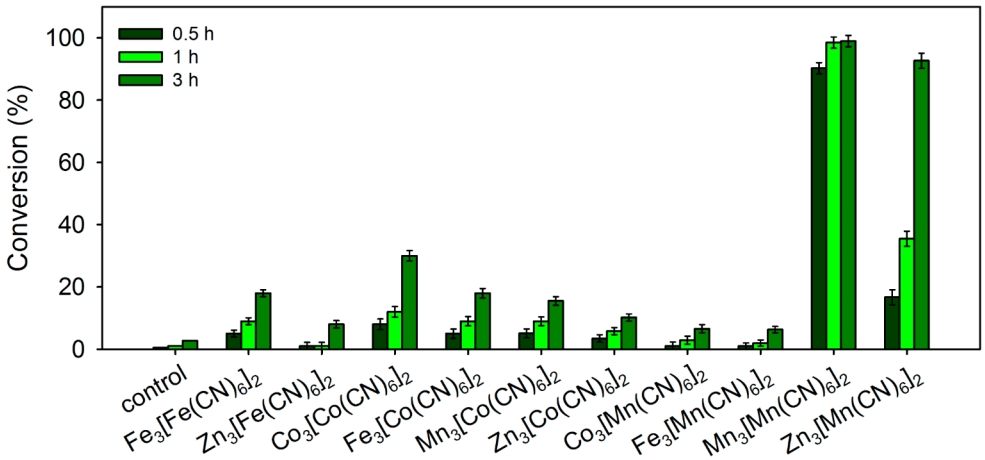

Fig. 2 Screening of various PBA catalysts for the ring-opening of CL. Reaction conditions: cat. loading = 0.3 mol%, EG = 0.9 mmol, CL = 9 mmol, T_p = 160 °C, t = 3 h

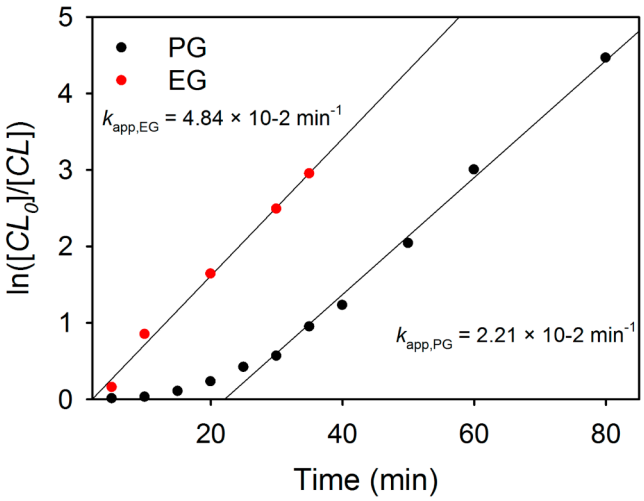

Fig. 3 Time-conversion plots of the ring-opening reaction of CL using EG or PG initiator and $Mn_3[Mn(CN)_6]_2$ catalyst. Reaction conditions: cat. loading = 0.3 mol%, initiator = 5 mmol, CL = 50 mmol

hydroxyl functional groups of EG and PG in the ring-opening of CL. Note that the ring opening of CL did not proceed in the absence of an initiator, as evidenced by the ^{1}H NMR spectra collected after 3 h of the reaction (Supplementary Fig. S16). The conversion of CL and the initiators over time was monitored using in situ ^{1}H NMR spectra collected at different intervals (Supplementary Figs. S17 and S18). The apparent rate constants (k_{app}) of the reactions were inferred from the plots of $\ln([CL_0]/[CL])$ versus time (Fig. 3). The linear relationship between $\ln([CL_0]/[CL])$ and time indicates that the ring opening of CL using the EG initiator is first-order with respect to the CL concentration, whereas the dependence on CL conversion in the reaction using the PG initiator was initially non-linear but transitioned to a linear regime at later stages. The deviation from this dependence after the early stages is attributed to the presence of both primary and secondary hydroxyl groups. The primary and secondary –OH groups were completely consumed after approximately 10 and 25 min, respectively, as evidenced by the disappearance of the ^{1}H NMR signals at 1.15, 3.39, and 3.91 ppm, corresponding to the methyl, methylene, and methine protons adjacent to the hydroxyl groups, respectively (Fig. 4). After complete consumption of the secondary OH groups, the ring opening of CL proceeded solely via the primary OH groups and followed a first-order reaction. The reaction conditions were optimized by varying the molar ratio of CL to PG. As shown in Fig. 5 and Supplementary Fig. S19, complete consumption of the secondary –OH group was achieved when the CL/PG ratio was equal to or greater than 3:1.

3.4 Synthesis of CL-terminated PPG Polyols

The ring-opening of CL using PPG was similar to that using PG, except that the content of secondary –OH groups in PPG was higher than that in PG (up to 95%). The former required a larger amount of CL to completely convert the secondary alcohols. Based on the kinetics data presented above, a series of CL-terminated PPG polyols was synthesized by varying the molar ratio of CL to PPG using $Mn_3[Mn(CN)_6]_2$ as the catalyst. A comparison of ^{1}H NMR spectra of PPG and the resulting CL-terminated PPG polyols is shown in Supplementary Fig. S20. The conversion of the CL and –OH groups of PPG at various CL/PPG ratios is reflected in the expanded NMR spectra in Fig. 6. Accordingly, signals corresponding to the methyl and methylene protons adjacent to the terminal –OH groups of PPG overlapped with those of the repeating units at approximately 1.08–1.18 ppm and 3.15–3.54 ppm, respectively, whereas signals related to the methine protons were observed at 3.93 ppm. After the reaction with CL, the methine signals of the proton were gradually depleted, while new signals appeared at 1.22 and 5.02 ppm, assigned to the methyl and methine protons, respectively, adjacent to the reacted terminal alcohols. The intensity of these signals increased in proportion to the CL/PPG ratio and reached a maximum when the CL/PPG ratio was equal to or higher than 5:1. The GPC curves of the resultant CL-capped PPG polyols exhibited a narrow MW distribution

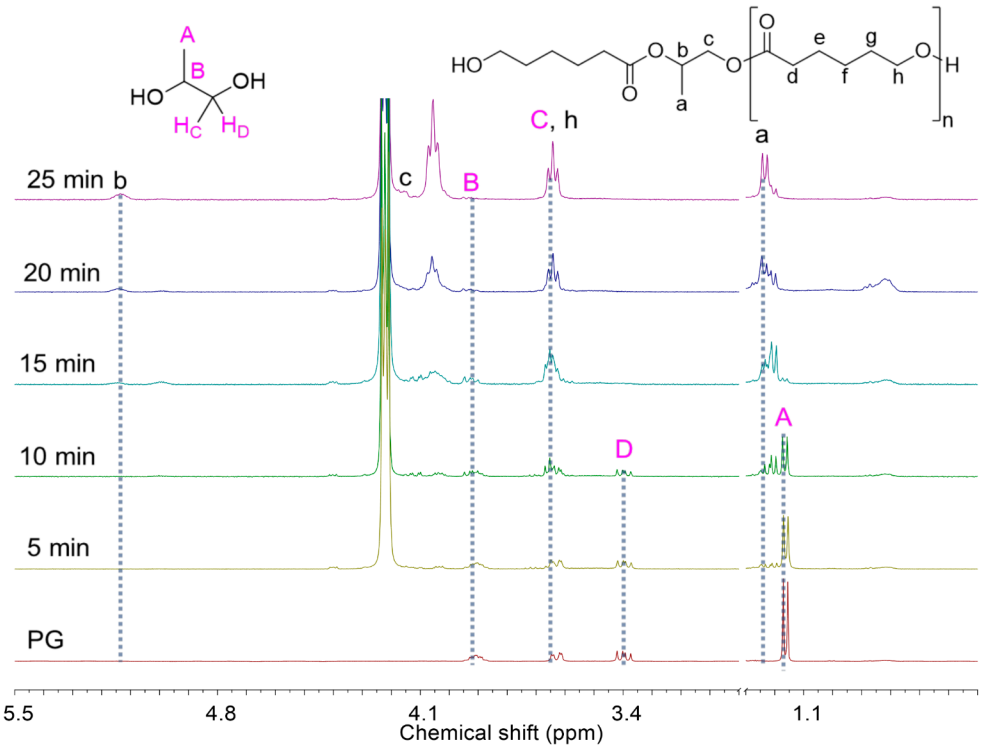

Fig. 4 Expanded in situ ^{1}H NMR (400 MHz, CD_3Cl_3) spectra of the crude reaction mixture in the ring-opening reaction of CL using PG and the $Mn_3[Mn(CN)_6]_2$ catalyst, acquired at the early stage of the reaction

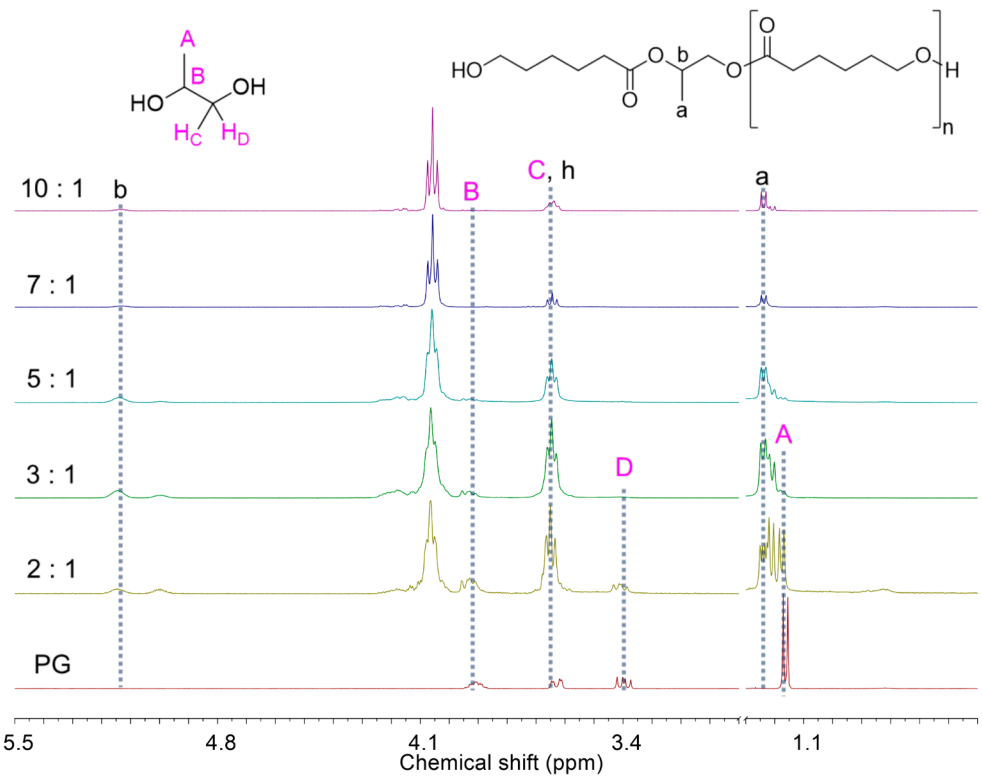

Fig. 5 Expanded ^{1}H NMR (400 MHz, CD_3Cl_3) spectra of the crude reaction mixture in the ring-opening reaction of CL using various molar ratios of CL to PG

(1.12–1.31), with MWs of 600–1800 g mol^{-1}, in good agreement with the calculated values (Supplementary Fig. S21). The results obtained in the synthesis of the CL-capped PPG polyols are summarized in Table 2.

The advantages of producing CL-terminated PPG polyols over conventional PPG were investigated using a model reaction in which HDI was used to synthesize polyurethane. The reactions were performed under vigorous stirring at 60 °C for 3 h in the absence of a catalyst. The reactions were monitored

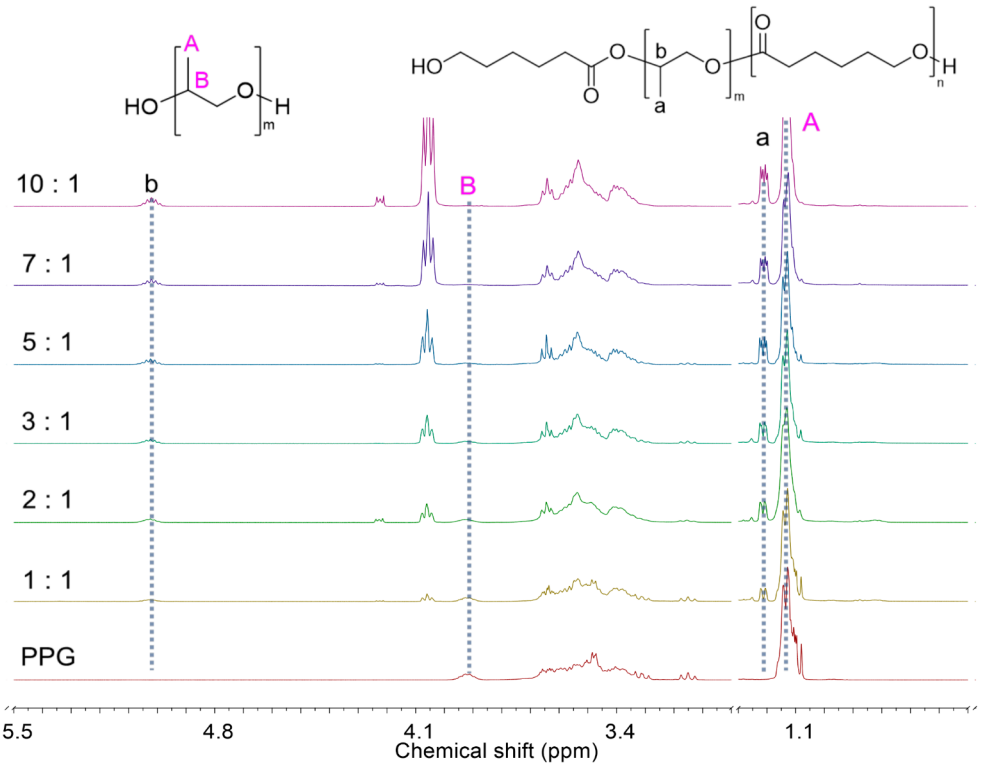

Fig. 6 Expanded ^{1}H NMR (400 MHz, CD_3Cl_3) spectra of the crude reaction mixture in the ring-opening reaction of CL using various CL: PPG ratios

Table 2 Results for the synthesis of CL-terminated PPG polyols

Polyol	CL/PPG ratio	t_p (min)	X_{CL} (%)	M_n			$Đ$
				Cal.	NMR	GPC	
PPG	–	–	–	500	–	560	1.08
PPG-CL1	1 : 1	70	94.87	614	941	600	1.12
PPG-CL2	2 : 1	80	96.79	728	777	800	1.19
PPG-CL3	3 : 1	120	94.93	842	842	900	1.26
PPG-CL5	5 : 1	120	94.84	1071	981	1200	1.30
PPG-CL7	7 : 1	120	98.55	1299	1520	1500	1.36
PPG-CL10	10 : 1	120	96.23	1641	1767	1800	1.31

Reaction conditions: cat. loading = 0.3 mol%, CL = 50 mmol, T_p = 160 °C

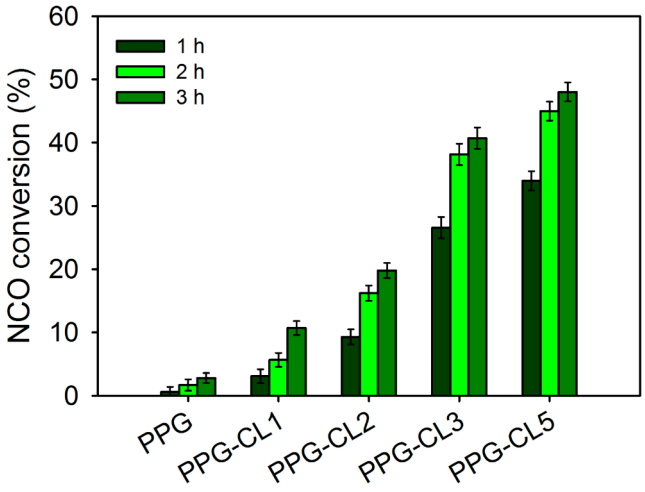

Fig. 7 Reactivity of CL-terminated PPG polyols with HDI. Reaction conditions: polyol = 5 g, HDI/polyol molar ratio = 2 : 1, T_p = 60 °C, t = 3 h

by in situ ^{1}H NMR analysis to determine the NCO conversion over time (Supplementary Figs. S22–S26). For conventional PPG, the signal assigned to the methylene protons adjacent to the –NCO groups at 3.32 ppm remained almost unchanged, indicating relatively poor reactivity for PU synthesis (NCO conversion of 2.7% after 3 h). As shown in Fig. 7, the NCO conversion increased in proportion to the CL/PPG ratio (from 10.7% for PPG-CL1 (CL/PPG = 1:1) to 41% for PPG-CL3 (CL/PPG = 3:1)) and reached a maximum of 48% at CL/PPG = 5:1 (PPG-CL5). The reactions were conducted without any catalyst, where an excess of HDI to polyol (HDI/polyol = 2:1) was used. The in situ FTIR spectra of the crude reaction mixture of PPG-CL and HDI were further investigated to corroborate the NMR data (Supplementary Figs. S27–S31). The consumption of NCO was monitored based on the reduction of the signals corresponding to the ν(–NCO) vibrations at approximately 2260 cm^{-1}. These results were in good agreement with the

NMR data, highlighting the superior reactivity of CL-capped polyols compared to conventional polyols.

4 Conclusions

A series of Prussian blue analogs catalysts was investigated for the synthesis of α,ω-primary hydroxyl-terminated polyols via the ring-opening reaction of ε-caprolactone. The $Mn_3[Mn(CN)_6]_2$ catalyst exhibited the highest activity and was used for further kinetic studies. The reactivity of the primary and secondary hydroxyls toward the ring opening of ε-caprolactone was determined using ethylene glycol and propylene glycol as representative initiators. The reaction using the ethylene glycol initiator proceeded via a simple coordinative mechanism with a first-order dependence on the ε-caprolactone concentration, whereas the reaction using the propylene glycol initiator was characterized by a two-stage kinetics plot. In the early stages, both the primary and secondary hydroxyl groups initiated the reaction. After complete consumption of the secondary hydroxyl groups, the reaction proceeded via a mechanism similar to that with the EG initiator. A ε-caprolactone/propylene glycol ratio of 3/1 was found to be suitable for the complete conversion of the secondary hydroxyls. Based on these findings, α,ω-primary hydroxyl-terminated polyols were successfully synthesized using polypropylene glycol as a macroinitiator. These polyols exhibited superior performance in polyurethane synthesis compared to the original polypropylene glycol, even in the absence of a catalyst. This work offers a promising approach for the synthesis of α,ω-primary hydroxyl-terminated precursors for a wide range of applications in the polyurethane industry.

Supplementary Information The online version contains supplementary material available at https://doi.org/10.1007/s11244-024-02007-6.

Acknowledgements This work was supported by a National Research Foundation of Korea (NRF) grant funded by the Korean government (MSIT) (2021R1A2C2003685) and partly supported by a Korea Institute of Energy Technology Evaluation and Planning (KETEP) grant funded by the Korean government (MOTIE) (20208401010080).

Authors contributions Chinh Hoang Tran: Conceptualization, Methodology, Validation, Formal Analysis, Investigation, Data Curation, Writing - Original Draft. Byeong-Ryeol Moon: Methodology, Formal Analysis, Investigation, Data Curation. Ju-Yeong Heo, So-Young Kim, Ji-Hwan Park, and Won-Seok Jae: Investigation, Formal Analysis and Data Curation. Il Kim: Conceptualization, Methodology, Data Curation, Writing - Review & Editing, Supervision, Funding acquisition, and correspondence.

Data Availability The datasets generated during and/or analysed during the current study are available from the corresponding author on reasonable request.

Declarations

Competing Interests The authors declare no conflicts of interest.

Supplementary Resources FTIR spectra, XRD patterns, TGA curves, and SEM images of the catalysts. NMR and FTIR spectroscopic data and GPC traces of the resulting products.

References

1. Tenorio-Alfonso A, Sánchez MC, Franco JM (2020) A review of the sustainable approaches in the production of bio-based polyurethanes and their applications in the Adhesive Field. J Polym Environ 28(3):749–774. https://doi.org/10.1007/s10924-020-01659-1
2. Bayer O (1947) Das Di-Isocyanat-Polyadditionsverfahren (polyurethane). Angew Chem A 59. https://doi.org/10.1002/ange.19470590901. :257 –272
3. Wicks ZW, Jones FN, Pappas SP, Wicks DA (2007) Organic Coatings: Science and Technology, Third edn. Wiley-Interscience, Hoboken, NJ
4. Meier-Westhues U (2007) Polyurethanes: Coatings, adhesives and sealants. Vincentz Network GmbH & Co KG, Hannover
5. Noreen A, Zia KM, Zuber M, Tabasum S, Zahoor AF (2016) Bio-based polyurethane: an efficient and environment friendly coating systems: a review. Prog Org Coat 91:25–32. https://doi.org/10.1016/j.porgcoat.2015.11.018
6. Llevot A, Meier M (2019) Perspective: green polyurethane synthesis for coating applications. Polym Int 68(5):826–831. https://doi.org/10.1002/pi.5655
7. Das A, Mahanwar P (2020) A brief discussion on advances in polyurethane applications. Adv Ind Eng Polym Res 3(3):93–101. https://doi.org/10.1016/j.aiepr.2020.07.002
8. Poussard L, Mariage J, Grignard B, Detrembleur C, Jérôme C, Calberg C, Heinrichs B, De Winter J, Gerbaux P, Raquez JM, Bonnaud L, Dubois P (2016) Non-isocyanate polyurethanes from carbonated soybean oil using Monomeric or Oligomeric diamines to achieve thermosets or thermoplastics. Macromolecules 49(6):2162–2171. https://doi.org/10.1021/acs.macromol.5b02467
9. Engels HW, Pirkl HG, Albers R, Albach RW, Krause J, Hoffmann A, Casselmann H, Dormish J (2013) Polyurethanes: versatile materials and sustainable problem solvers for today's challenges. Angew Chem Int Ed 52(36):9422–9441. https://doi.org/10.1002/anie.201302766
10. Al-Homoud MS (2005) Performance characteristics and practical applications of common building thermal insulation materials. Build Environ 40(3):353–366. https://doi.org/10.1016/j.buildenv.2004.05.013
11. Statista (2023) Market volume of polyurethane worldwide from 2015 to 2025, with a forecast for 2022 to 2029. https://www.statista.com/statistics/720341/global-polyurethane-market-size-forecast/
12. de Souza FM, Kahol PK, Gupta RK (2021) Introduction to Polyurethane Chemistry. In: Polyurethane Chemistry: Renewable Polyols and Isocyanates, vol 1380. ACS Symposium Series, vol 1380. American Chemical Society, pp 1–24. https://doi.org/10.1021/bk-2021-1380.ch001
13. Saunders JH, Frisch KC (1962) Polyurethanes: Chemistry and Technology. Vol pt, vol 1. Interscience, New York, USA
14. Penczek S, Cypryk M, Duda A, Kubisa P, Słomkowski S (2007) Living ring-opening polymerizations of heterocyclic monomers. Prog Polym Sci 32(2):247–282. https://doi.org/10.1016/j.progpolymsci.2007.01.002

15. Miyajima T, Nishiyama K, Satake M, Tsuji T (2015) Synthesis and process development of polyether polyol with high primary hydroxyl content using a new propoxylation catalyst. Polym J 47(12):771–778. https://doi.org/10.1038/pj.2015.64
16. Herold RJ, Livigni RA (1973) Hexacyanometalate Salt Complexes as catalysts for Epoxide Polymerizations. Polymerization kinetics and technology. Advances in Chemistry, vol 128. vol 128. American Chemical Society, pp 208–229. doi:https://doi.org/10.1021/ba-1973-0128.ch015
17. Kim I, Ahn J-T, Ha CS, Yang CS, Park I (2003) Polymerization of propylene oxide by using double metal cyanide catalysts and the application to polyurethane elastomer. Polymer 44(11):3417–3428. https://doi.org/10.1016/S0032-3861(03)00226-X
18. Chakraborty D, Rodriguez A, Chen EYX (2003) Catalytic Ring-opening polymerization of propylene oxide by Organoborane and Aluminum Lewis acids. Macromolecules 36(15):5470–5481. https://doi.org/10.1021/ma034050a
19. Erker G (2005) Tris(pentafluorophenyl)borane: a special boron Lewis acid for special reactions. Dalton Trans 111883–1890. https://doi.org/10.1039/B503688G
20. Herzberger J, Niederer K, Pohlit H, Seiwert J, Worm M, Wurm FR, Frey H (2016) Polymerization of ethylene oxide, propylene oxide, and other alkylene oxides: synthesis, novel polymer architectures, and bioconjugation. Chem Rev 116(4):2170–2243. https://doi.org/10.1021/acs.chemrev.5b00441
21. Kaushiva BD (2005) Single reactor synthesis of KOH-capped polyolsbased on DMC-synthesized intermediates. US Patent US2005/0096488A1, May 5, 2005
22. Raghuraman A, Babb D, Miller M, Paradkar M, Smith B, Nguyen A (2016) Sequential DMC/FAB-Catalyzed alkoxylation toward high primary hydroxyl, high Molecular Weight Polyether Polyols. Macromolecules 49(18):6790–6798. https://doi.org/10.1021/acs.macromol.6b01363
23. Shi J, Shi Z, Yan H, Wang X, Zhang X, Lin Q, Zhu L (2018) Synthesis of Zn–Fe double metal cyanide complexes with imidazolium-based ionic liquid cocatalysts via ball milling for copolymerization of CO_2 and propylene oxide. RSC Adv 8(12):6565–6571. https://doi.org/10.1039/C7RA12528C
24. An N, Li Q, Yin N, Kang M, Wang J (2018) Effects of Addition Mode on Zn–Co double metal Cyanide Catalyst for Synthesis of Oligo(Propylene-Carbonate) Diols. Appl Organomet Chem 32(11):e4509. https://doi.org/10.1002/aoc.4509
25. Sebastian J, Srinivas D (2011) Novel application of a Fe–Zn double-metal Cyanide Catalyst in the synthesis of biodegradable, hyperbranched polymers. Chem Commun 47(37):10449–10451. https://doi.org/10.1039/C1CC13443D
26. Gu Y, Dong X (2013) Novel application of double metal cyanide in the synthesis of Hyperbranched Polyether Polyols. Des Monomers Polym 16(1):72–78. https://doi.org/10.1080/15685551.2012.705492
27. Tran CH, Lee MW, Kim SA, Jang HB, Kim I (2020) Kinetic and mechanistic study of heterogeneous double metal cyanide-catalyzed Ring-opening multibranching polymerization of Glycidol. Macromolecules 53(6):2051–2060. https://doi.org/10.1021/acs.macromol.9b02373
28. Liu Z-H, Li Y, Zhang C-J, Zhang Y-Y, Cao X-H, Zhang X-H (2020) Synthesis of high-molecular-weight poly(ε-caprolactone) via heterogeneous zinc-cobalt(III) double metal cyanide complex. Giant 3:100030. https://doi.org/10.1016/j.giant.2020.100030
29. Tran CH, Lee M-W, Lee S-J, Choi J-H, Lee E-G, Choi H-K, Kim I (2022) Highly active heterogeneous double metal cyanide catalysts for Ring-opening polymerization of cyclic monomers. Polymers 14(12):2507. https://doi.org/10.3390/polym14122507
30. Tran CH, Choi H-K, Lee E-G, Moon B-R, Song W, Kim I (2023) Prussian blue analogs as catalysts for the fixation of CO_2 to glycidol to produce glycerol carbonate and multibranched polycarbonate polyols. J CO2 Util 74:102530. https://doi.org/10.1016/j.jcou.2023.102530
31. Tran CH, Kim S, Choi H-K, Moon B-R, Song W, Yeong Heo J, Kim I (2024) Multi-role heterogeneous Zn–Co double metal cyanide catalysts valid for ring-opening polymerizations and hydrofunctionalizations. J Ind Eng Chem. https://doi.org/10.1016/j.jiec.2024.03.039
32. Liu Q, Hu Z, Chen M, Zou C, Jin H, Wang S, Chou S-L, Liu Y, Dou S-X (2020) The Cathode choice for commercialization of Sodium-Ion batteries: layered transition metal oxides versus prussian blue analogs. Adv Funct Mater 30(14):1909530. https://doi.org/10.1002/adfm.201909530
33. Wang X, Roy S, Shi Q, Li Y, Zhao Y, Zhang J (2021) Progress in and application prospects of advanced and cost-effective iron (Fe)-based cathode materials for sodium-ion batteries. J Mater Chem A 9(4):1938–1969. https://doi.org/10.1039/D0TA10610K
34. Xu D, Wang W, Zhu M, Li C (2020) Recent advances in Desalination Battery: an initial review. ACS Appl Mater Interfaces 12(52):57671–57685. https://doi.org/10.1021/acsami.0c15413
35. Xiao J, Li X, Tang K, Wang D, Long M, Gao H, Chen W, Liu C, Liu H, Wang G (2021) Recent progress of emerging cathode materials for sodium ion batteries. Mater Chem Front 5(10):3735–3764. https://doi.org/10.1039/D1QM00179E
36. Chen C, Shi F, Xu Z-L (2021) Advanced electrode materials for nonaqueous calcium rechargeable batteries. J Mater Chem A 9(20):11908–11930. https://doi.org/10.1039/D1TA00757B
37. Reddy RCK, Lin J, Chen Y, Zeng C, Lin X, Cai Y, Su C-Y (2020) Progress of nanostructured metal oxides derived from metal–organic frameworks as anode materials for lithium–ion batteries. Coord Chem Rev 420:213434. https://doi.org/10.1016/j.ccr.2020.213434
38. Zampardi G, La Mantia F (2020) Prussian blue analogues as aqueous Zn-ion batteries electrodes: current challenges and future perspectives. Curr Opin Electrochem 21:84–92. https://doi.org/10.1016/j.coelec.2020.01.014
39. Yan J, Ang EH, Yang Y, Zhang Y, Ye M, Du W, Li CC (2021) High-voltage zinc-ion batteries: Design Strategies and challenges. Adv Funct Mater 31(22):2010213. https://doi.org/10.1002/adfm.202010213
40. Ma L, Cui H, Chen S, Li X, Dong B, Zhi C (2021) Accommodating diverse ions in prussian blue analogs frameworks for rechargeable batteries: the electrochemical redox reactions. Nano Energy 81:105632. https://doi.org/10.1016/j.nanoen.2020.105632
41. Zhou A, Cheng W, Wang W, Zhao Q, Xie J, Zhang W, Gao H, Xue L, Li J (2021) Hexacyanoferrate-type prussian blue analogs: principles and advances toward high-performance Sodium and Potassium Ion Batteries. Adv Energy Mater 11(2):2000943. https://doi.org/10.1002/aenm.202000943
42. Busquets MA, Estelrich J (2020) Prussian blue nanoparticles: synthesis, surface modification, and biomedical applications. Drug Discov Today 25(8):1431–1443. https://doi.org/10.1016/j.drudis.2020.05.014
43. Wang X, Cheng L (2020) Multifunctional prussian blue-based nanomaterials: Preparation, modification, and theranostic applications. Coord Chem Rev 419:213393. https://doi.org/10.1016/j.ccr.2020.213393
44. Gao Y, Yu G, Xing K, Gorin D, Kotelevtsev Y, Tong W, Mao Z (2020) Finely tuned prussian blue-based nanoparticles and their application in disease treatment. J Mater Chem B 8(32):7121–7134. https://doi.org/10.1039/D0TB01248C
45. Matos-Peralta Y, Antuch M (2019) Review—prussian blue and its analogs as appealing materials for Electrochemical Sensing and Biosensing. J Electrochem Soc 167(3):037510. https://doi.org/10.1149/2.0102003JES
46. Lee PK, Woi PM (2020) Current innovations of metal hexacyanoferrates-based nanocomposites toward Electrochemical sensing:

materials selection and synthesis methods. Crit Rev Anal Chem 50(5):393–404. https://doi.org/10.1080/10408347.2019.1642733
47. Karpova EV, Karyakin AA (2020) Noninvasive monitoring of diabetes and hypoxia by wearable flow-through biosensors. Curr Opin Electrochem. https://doi.org/10.1016/j.coelec.2020.02.018. 23:16–20
48. Estelrich J, Busquets MA (2021) Prussian Blue: a safe pigment with Zeolitic-Like Activity. Int J Mol Sci 22(2):780
49. Zhao Z, Xiong Y, Cheng X, Hou X, Yang Y, Tian Y, You J, Xu L (2020) Adsorptive removal of trace thallium(I) from wastewater: a review and new perspectives. J Hazard Mater 393:122378. https://doi.org/10.1016/j.jhazmat.2020.122378
50. Lee E-G, Tran CH, Heo J-Y, Kim S-Y, Choi H-K, Moon B-R, Kim I (2024) Synthesis of Polyether, Poly(Ether Carbonate) and poly(Ether Ester) polyols using double metal cyanide catalysts bearing Organophosphorus Complexing agents. Polymers 16(6):818. https://doi.org/10.3390/polym16060818
51. Adamson AW, Welker JP, Wright W (1951) Exchange studies with Complex ions. II. The kinetics of the Exchange of Radiocyanide Ion with Potassium Hexacyanomanganate (III) in aqueous Solution1. J Am Chem Soc 73(10):4786–4790. https://doi.org/10.1021/ja01154a092
52. Peixoto DA, Silva SC, Borges PHS, Lima RC, Nossol E (2023) Hydrothermal synthesis as a versatile tool for the preparation of metal hexacyanoferrates: a review. J Mater Sci 58(7):2993–3024. https://doi.org/10.1007/s10853-023-08190-3